

ORIGINAL ARTICLE

Nanoscopy reveals surface-metallic black phosphorus

Yohannes Abate^{1,2}, Sampath Gamage², Zhen Li³, Viktoriia Babicheva^{1,2}, Mohammad H Javani^{1,2}, Han Wang³, Stephen B Cronin³ and Mark I Stockman^{1,2}

Black phosphorus (BP) is an emerging two-dimensional material with intriguing physical properties. It is highly anisotropic and highly tunable by means of both the number of monolayers and surface doping. Here, we experimentally investigate and theoretically interpret the near-field properties of a-few-atomic-monolayer nanoflakes of BP. We discover near-field patterns of bright outside fringes and a high surface polarizability of nanofilm BP consistent with its surface-metallic, plasmonic behavior at mid-infrared frequencies $< 1176\text{ cm}^{-1}$. We conclude that these fringes are caused by the formation of a highly polarizable layer at the BP surface. This layer has a thickness of $\sim 1\text{ nm}$ and exhibits plasmonic behavior. We estimate that it contains free carriers in a concentration of $n \approx 1.1 \times 10^{20}\text{ cm}^{-3}$. Surface plasmonic behavior is observed for 10–40 nm BP thicknesses but absent for a 4-nm BP thickness. This discovery opens up a new field of research and potential applications in nanoelectronics, plasmonics and optoelectronics.

Light: Science & Applications (2016) 5, e16162; doi:10.1038/lssa.2016.162; published online 21 October 2016

Keywords: black phosphorus; infrared spectroscopy; metallic surface layer; near-field nanoscopy; two-dimensional materials

INTRODUCTION

Nanolayered and two-dimensional (2D) materials¹ such as graphene^{2,3}, boron nitride^{1,4}, transition metal dichalcogenides^{1,5–8} (TMDCs) and black phosphorus (BP)^{1,9–13} have intriguing physical properties and bear the promise of important applications^{9,14,15}. Among them, BP^{11,12,16} has unique electronic properties because of its anisotropic structure. The advantages of BP in nanoelectronics and nano-optics arise from the fact that its carrier density can be dynamically controlled via gating, as in field-effect transistors (FETs)^{9,14,15}. However, the near-field properties of BP have not yet been investigated experimentally. Here, we report the first observation of the nanoscopic near-field properties of BP. We have discovered near-field patterns of bright outside fringes and a high-surface polarizability of nanofilm BP consistent with its surface-metallic, plasmonic behavior at mid-infrared (mid-IR) frequencies below $\omega_m \approx 1176\text{ cm}^{-1}$. This has allowed us to estimate plasma frequency of $\hbar\omega_p \approx 0.4\text{ eV}$, a carrier density of $n \approx 1.1 \times 10^{20}\text{ cm}^{-3}$ and a surface metallic layer thickness of $\sim 1\text{ nm}$. We have also observed similar behavior in other nanolayer semiconductors, such as TMDC MoS₂ and topological insulator Bi₂Te₃ but not in insulators such as boron nitride. Surface plasmonic behavior is observed for 10–40 nm BP thicknesses, but it disappears for a 4-nm BP thickness. Our findings open up a new avenue of research and suggest potential applications in nanoelectronics, plasmonics and optoelectronics.

In contrast to graphene, a semimetal, BP is a semiconductor whose band gap depends on the number of atomic layers and, for a thickness of $\geq 10\text{ nm}$, is $\sim 0.3\text{--}0.4\text{ eV}$ ^{17,18}, that is, smaller than that of TMDCs. In contrast to multilayer TMDCs, which have indirect band gaps, BP

exhibits direct band gap properties regardless of its thickness, which is a significant advantage for optoelectronic applications. In addition, BP has a rather high carrier mobility ($\sim 200\text{--}1000\text{ cm}^2\text{ V s}^{-1}$)^{19,20}, high on/off ratios in transistors^{9,14}, strong excitonic effects and strongly anisotropic optical, electrical and thermal conductances²⁰, which can be attributed to its puckered crystalline structure. These physical properties can be manipulated by altering its layer thickness¹⁸, its stacking order²¹, the applied strain force²² and the external electric field²³, offering tremendous advantages for using BP in numerous potential applications in optics and electronics. The carrier density of the anisotropic thin-film BP can be manipulated by modifying the doping levels of the BP nanolayers, allowing excellent control of the interaction of BP with light²⁴.

MATERIALS AND METHODS

Near-field microscopy

The microscope used in this study is a commercial s-SNOM system (neaspec.com). A probing linearly p-polarized quantum cascade laser is focused on the tip-sample interface at an angle of 45° to the sample surface. The scattered field is acquired through phase-modulation (pseudoheterodyne) interferometry. The background signal is suppressed by vertical tip oscillations at the mechanical resonance frequency of the cantilever ($f_0 \sim 285\text{ kHz}$) and demodulation of the detector signal at higher harmonics nf_0 (commonly $n = 2, 3, 4$) of the tip resonance frequency. The combined scattered fields from the tip and the reference beam pass through a linear polarizer, which further selects the p-polarized excitation and p-polarized detection signal for analysis.

¹Center for Nano-Optics, Georgia State University, Atlanta, GA 30303, USA; ²Department of Physics and Astronomy, Center for Nano-Optics, Georgia State University, Atlanta, GA 30303, USA and ³Viterbi School of Engineering, University of Southern California, Los Angeles, CA 90089, USA

Correspondence: Y Abate, E-mail: yabate@gsu.edu; MI Stockman, E-mail: mstockman@gsu.edu

Received 9 December 2015; revised 22 April 2016; accepted 6 May 2016; accepted article preview online 9 May 2016

Sample fabrication

BP flakes were exfoliated by means of mechanical exfoliation onto oxidized silicon wafers. Thin coatings of Al_2O_3 were deposited via atomic layer deposition at 220 °C with trimethyl aluminum as the Al source and water vapor as the oxygen source.

RESULTS AND DISCUSSION

Here, we report the first experimental near-field optical nanoscopic investigation of BP at mid-IR frequencies. We have observed near-field amplitude patterns, which allow direct imaging of the gap field at the tip-sample junction via bright fringes formed at the BP edges outside of the geometric boundaries of the BP. Based on a comparison with the results of full electrodynamic modeling, we attribute these

observations to a high-surface polarizability of the BP, consistent with surface-metallic, plasmonic behavior at mid-IR frequencies. Note that such surface charging is a well-known phenomenon in conventional 3D semiconductors²⁵ but has never been previously reported for BP or other nanolayer materials.

Near-field optical images were acquired using a commercial s-SNOM system, represented schematically in Figure 1a. A linearly polarized mid-IR quantum cascade laser (Daylight Solutions) is focused on the tip-sample interface at an angle of 45° to the sample surface, and the scattered field is detected by phase-modulation interferometry. Topographic (Figure 1c) and third-harmonic near-field amplitude images of a wedge-shaped uncoated BP exfoliated flake on a Si/SiO_2 substrate at two frequencies (Figure 1d and 1e) are

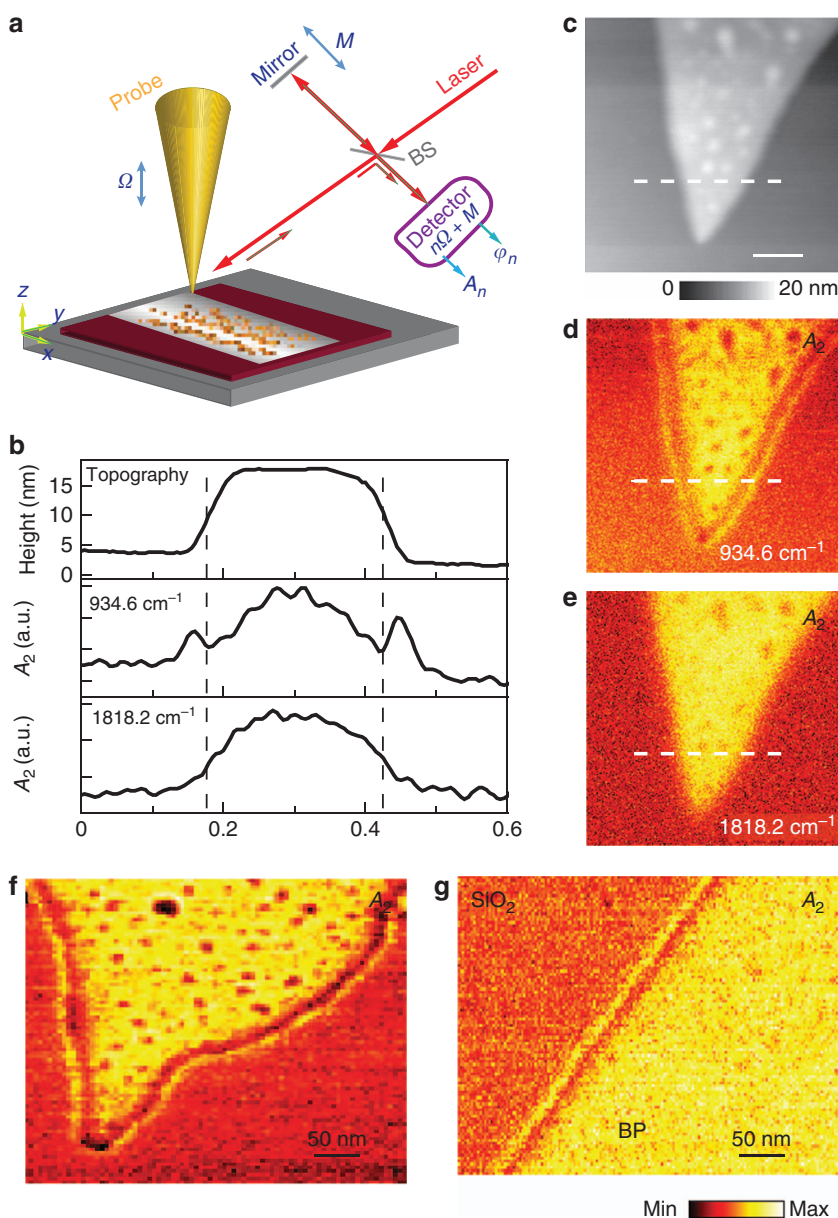


Figure 1 Edge fringe nanoscopy. (a) Experimental schematic. (b) Line profiles, where the dashed lines represent the physical boundaries of the BP. (c) Topographic image. (d, e) Near-field amplitude images of uncoated BP at two frequencies: (d) $\omega = 934.6 \text{ cm}^{-1}$, showing a bright-contrast fringe enclosing the edge of the BP, and (e) $\omega = 1818.2 \text{ cm}^{-1}$, showing the absence of a fringe. (f) Bare BP and (g) BP of similar thickness coated with 1 nm of Al_2O_3 . The small dark spots in the images of the uncoated samples c–f are the result of degradation (oxidation) of the BP.

shown. The near-field amplitude images displayed in Figure 1d and 1e show bright contrast compared with the substrate. The amplitude image acquired at $\omega = 934.6 \text{ cm}^{-1}$ (Figure 1d) shows a bright fringe surrounding the wedge, separated from the inner bright surface of the structure by a region of dark contrast. Such an edge fringe is missing in the near-field amplitude image acquired at $\omega = 1818.2 \text{ cm}^{-1}$ (Figure 1e), suggesting a strong frequency dependence of fringe formation. In fact, the fringe disappears at a critical frequency of $\omega_m \approx 1176 \text{ cm}^{-1}$.

The observed fringe in Figure 1d is situated strictly outside the geometric limits of the BP structure, as shown by the straight dashed lines drawn across the line profile plots of the three images shown in Figure 1b. Similar bright outside fringes followed by a dark-contrast fringe are seen in Figure 1g for BP coated with 1 nm Al_2O_3 and in Figure 1f for uncoated BP of the identical thickness.

We associate this outside fringe around the BP nanoflake with a high surface polarizability related to its metallic, plasmonic behavior. Note that a metal nanolayer at the surface of BP was recently observed²⁶ using angle-resolved photoelectron spectroscopy. However, in ref 26, the BP was heavily doped with potassium. By contrast, the BP investigated in the present work is nominally undoped.

In our case, the frequency $\omega_m \approx 1176 \text{ cm}^{-1}$ at which the fringe disappears is the surface plasmon frequency, which corresponds to the dielectric permittivity²⁷ $\epsilon_{\text{SP}} = -1$. We will use the Drude formula, $\epsilon = \epsilon_0 - (\omega_p/\omega)^2$, where ω_p is the bulk plasma frequency of the surface layer and ϵ_0 is the background (high-frequency) permittivity. Setting $\epsilon_0 = 6$, as a typical value for narrow-band semiconductors, we obtain $\omega_p = \omega_m \sqrt{\epsilon_0 - \epsilon_{\text{SP}}} \approx 0.4 \text{ eV} \approx 3224 \text{ cm}^{-1}$. From this, we find the 3D electron density, $n = m_e \omega_p^2 / (4\pi e^2) \approx 1.1 \times 10^{20} \text{ cm}^{-3}$, where e is unit charge and m_e is electron mass, which is a density that is reasonable for highly doped conducting semiconductors exhibiting plasmonic behavior²⁸. These high-density charges are likely to originate from the band bending caused by the surface dopants, as is known for conventional 3D semiconductors²⁵. Such charges form a ‘metallic’ surface layer, the thickness of which can be estimated as the corresponding Thomas–Fermi screening length, $r_{\text{TF}} = \hbar \epsilon_{\text{BP}}^{1/2} (2e)^{-1} m_e^{-1/2} (3n/\pi)^{-1/6} \sim 1 \text{ nm}$, where ϵ_{BP} is the bulk permittivity of BP (we set $\epsilon_{\text{BP}} = 6$, the same as ϵ_0 above).

The optical phonon frequencies of the SiO_2 substrate in our spectral range are from 797 cm^{-1} to 1129 cm^{-1} , of which optical transverse phonons at a frequency of $\omega_{\text{TO}} = 1163 \text{ cm}^{-1}$ and longitudinal optical phonons at $\omega_{\text{LO}} = 1165 \text{ cm}^{-1}$ produce the strongest near-field responses²⁹. In silica, a broad phonon line at $\omega_{\text{O}} \approx 1130 \text{ cm}^{-1}$ dominates²⁹. We have not seen any evidence that the substrate phonons affect the observed near-field images. The reason may be that these images originate from the upper surface of the BP, which is $\sim 10\text{--}20 \text{ nm}$ away from the substrate. In contrast, for graphene, strong hybridization of the substrate optical phonons with the graphene plasmons has been observed^{30,31}. No quenching of surface plasmons by optical phonons has been found. Thus, the similarity in value between ω_m and ω_{O} is a pure coincidence. Additional evidence of the absence of any appreciable effect of the substrate is provided by the fact that an identical outside fringe is also observed with other substrates, namely, BP (Supplementary Fig. S4), and sapphire and GaAs (data not shown); see also Figure 3 and its accompanying discussion below.

With the electron density of $n \sim 1 \times 10^{20} \text{ cm}^{-3}$, the Thomas–Fermi screening radius is $\sim 1 \text{ nm}$, suggesting that there is a metallic nanolayer at the surface of the BP. Assuming the presence of such a surface layer, we performed full electrodynamic modeling of the near fields using time-domain software from both Lumerical (Vancouver, BC, Canada)

and CST Microwave Studio (Framingham, MA, USA), obtaining consistent results with both (see also Supplementary Fig. S1). As Figure 2b–2d show, when the s-SNOM tip is close to the edge of the sample, a gap hot-spot field is produced between the tip and the sample edge, reminiscent of hot spots in metal nanoplasmonics³². The field in the hot spot depends on the permittivity of the sample surface—see Figure 2a. A bright fringe followed by a region of dark contrast that precedes a bright area on the sample surface is formed when a metallic layer ($\text{Re}\epsilon < 0$, which is a requirement for plasmonicity²⁷) is present at the surface. The contrast of the outside fringe increases with increasing $-\text{Re}\epsilon$, consistent with a plasmonic high polarizability of the sample surface. The best reproduction of the experimental data at a frequency of $\omega = 934.6 \text{ cm}^{-1} \approx 0.116 \text{ eV}$ is obtained for $\epsilon = -5 + i0.5$. From this value, employing the Drude formula, we again independently determine the plasma frequency, obtaining $\omega_p = \omega \sqrt{\epsilon_0 - \text{Re}\epsilon(\omega)} \approx 0.4 \text{ eV}$, which is fully consistent with the value of $\approx 0.4 \text{ eV}$ obtained above from the frequency ω_m at which the fringe experimentally disappears. Note that if the edge of the sample were not sharp as in Figure 2b–2e, our simulations show that the outside fringe would disappear. This explains why this outside fringe has never been seen in metal plasmonics, where the edges of the metal nanostructures are not sufficiently sharp.

The hot spots seen in Figure 2 are regions of high intensity of the local field that is electro-dynamically coupled to the vertical (along the probe axis) polarization of the external field. Note that the local field at the apex is polarized normally to the surface, almost radially; it corresponds to an electric charge that is displaced to the apex, oscillating at the optical frequency. Therefore, hot spots are produced both when the tip is above the surface and when it is to the side of the sharp edge, as seen in Figure 2b–2d and Supplementary Fig. S1a–S1c.

The coupling of the external field to the hot spots also works in reverse (electrodynamics is fully reversible): if the vertical external field excites a hot spot, then the field of this hot spot will be scattered by the tip into the external far field. Thus, this scattering into the far field will produce similar images of the fringes seen in the near field. This is also strongly supported by the fact that the intensity of the near field and the power dissipated from the far field are very similarly distributed in space—see Supplementary Fig. S1d and S1e.

Spatially, the bright fringe is detected to lie outside of the edge of the BP by a distance approximately equal to the radius of curvature of the apex of the s-SNOM tip, which is $\sim 20 \text{ nm}$. This is in good qualitative agreement with the experimental near-field images shown in Figure 1d–1g. The edge of the nanosystem should be sufficiently sharp to produce the bright fringe—see Supplementary Fig. S2 and its accompanying discussion.

For a metallic nanofilm, the dispersion relation for surface plasmon polaritons (SPPs) is³³ $k(\omega) = (\epsilon_1 + \epsilon_2) / [a\epsilon(\omega)]$, where $k(\omega)$ is the wave vector; ϵ_1 and ϵ_2 are the permittivities of the substrate and superstrate, respectively; $\epsilon(\omega)$ is the permittivity of the metallic layer on the BP at observation frequency ω ; and $a \sim r_{\text{TF}} \sim 1 \text{ nm}$ is the thickness of the metallic layer. For $\epsilon = -5 + i0.5$ at $\omega = 934.6 \text{ cm}^{-1}$, $\epsilon_1 = 6$ (inside the BP nanolayer) and $\epsilon_2 = 1$ (vacuum), we find that the SPP wavelength is $\lambda_{\text{SPP}} = 2\pi/\text{Re}k = 2.2 \text{ nm}$ and the decay length is $1/(2\text{Im}k) = 2.1 \text{ nm}$. Both of these lengths are too small to be resolved by our s-SNOM system. This explains why no fringes are seen in our spatial scans of the BP.

To further elucidate the frequency dependence of the observed edge fringe contrast in Figures 1 and 2 and reconfirm its dependence on the plasmonic behavior of the BP, we performed spectroscopic imaging of a BP nanolayer at a series of frequencies. The thickness of the BP sample was $h \sim 20 \text{ nm}$ (topography shown in Figure 3a), with a

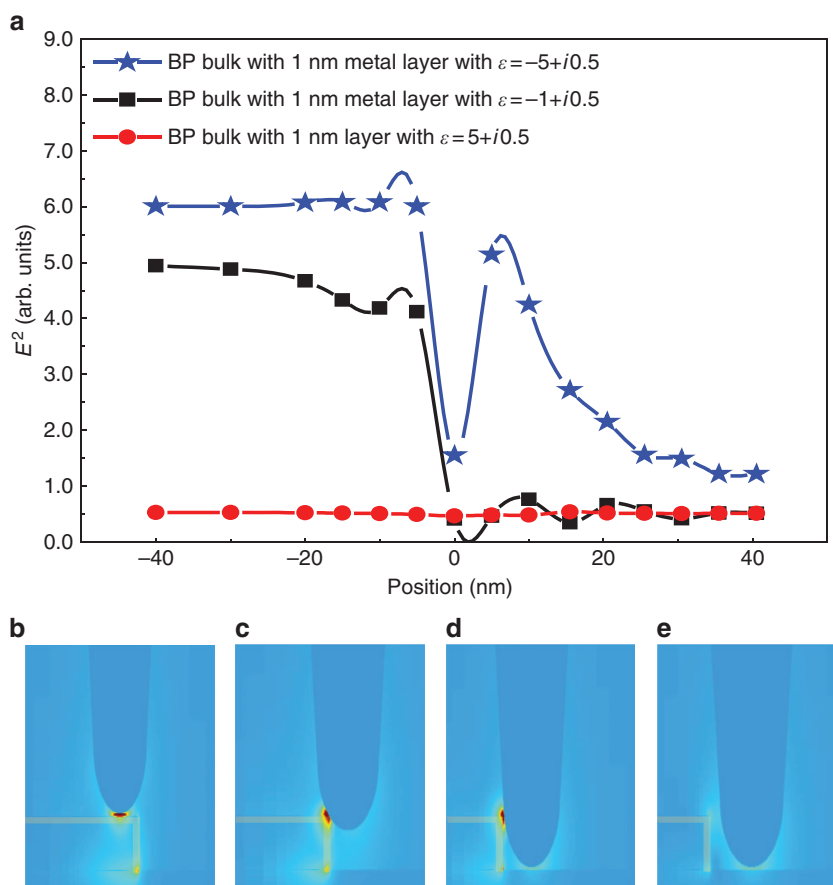


Figure 2 Theoretical simulations of edge fringe formation. **(a)** Theoretical simulations calculating the near field between the tip and the BP as a function of the tip position for 1 nm metallic layers at the BP surface indicated by the shadowed areas in yellow. The calculations were performed for the metal permittivities ϵ indicated in the panel. **(b–e)** Near-field amplitude distributions for $\epsilon = -5 + i0.5$ for the tip positions shown.

~ 1 nm coating of Al_2O_3 to inhibit oxidation degradation. Figure 3b shows a plot of the normalized fourth-harmonic near-field amplitude for exfoliated BP on a SiO_2 substrate as a function of excitation frequency. As shown in Figure 3b, for the frequency range between 1000 cm^{-1} and 1200 cm^{-1} , the normalized amplitude signal is < 1 (dark contrast of BP with respect to the substrate, which is associated with the known Reststrahlen effect in silica), whereas for all other frequencies, the normalized amplitude value is > 1 (bright contrast of BP with respect to the substrate). This plot indicates highly frequency-dependent near-field contrast formation of the edge fringe for BP, observed here for the first time.

In Figure 3c–3e, we show optical near-field amplitude images taken at three select frequencies included in the plot presented in Figure 3b. These images faithfully represent this plot by showing a BP contrast darker than the substrate for $\omega = 1176.6\text{ cm}^{-1}$ (Figure 3c) and $\omega = 1052.6\text{ cm}^{-1}$ (Figure 3d), which implies a smaller real part of the BP permittivity compared with that of SiO_2 . For $\omega = 934.6\text{ cm}^{-1}$ (Figure 3e), the BP surface is brighter than the substrate, indicating a larger $|\text{Re}\epsilon|$ of the BP compared with that of the SiO_2 substrate. Moreover, the fringe around the nanostructured BP is clearly visible at $\omega = 934.6\text{ cm}^{-1}$ (Figure 3e) and disappears at $\omega = 1176.6\text{ cm}^{-1}$ (Figure 3c). At $\omega = 1052.6\text{ cm}^{-1}$ (Figure 3d), the BP brightness is low compared with that of the SiO_2 substrate, yet the fringe around the BP is discernible. This frequency lies within the phonon (Reststrahlen) band of SiO_2 (see, for example, ref. 29.) and also within the plasmonic region of BP; thus, this observation of a bright fringe

directly demonstrates that the optical phonons of the substrate do not suppress the plasmonic behavior of the BP.

To test the universal nature of the observed outside-fringe formation, which we observe to occur for sharp-edged semiconductor nanolayers exhibiting surface-metallic behavior, we performed similar experiments using several nanolayered materials on identical SiO_2 substrates imaged at 934.5 cm^{-1} , where the strongest fringe contrast was found for BP. As shown in Figure 4, we observe a similar, albeit weaker, edge fringe for other nanolayered materials: a TMDC semiconductor, MoS_2 (Figure 4a), and a narrow-band gap topological insulator, Bi_2Te_3 (Figure 4b), which are of similar height ($h \sim 20$ nm), which is suggestive of plasmonic behavior. In contrast, an image of the dielectric h-BN shows no fringes at $\omega = 934.6\text{ cm}^{-1}$ (Figure 4d), a behavior that is expected for an insulator with no electronic plasmonic response. However, when tuned to a frequency in the phonon-polariton (Reststrahlen) spectral range, $\omega = 1562.5\text{ cm}^{-1}$ (Figure 4c), h-BN shows the expected fringes inside the structure (Figure 4c), in agreement with recent observations³⁴.

Non-encapsulated BP nanofilms chemically degrade (oxidize) under ambient conditions³⁵. We investigated the effect of degradation on the observed surface-metallic behavior by imaging a bare (unprotected) exfoliated BP sample left in air to degrade for several weeks. We performed near-field optical amplitude imaging at two frequencies, one where a strong fringe is expected in native BP ($\omega = 934.6\text{ cm}^{-1}$) and a higher frequency above the ω_m plasmonic edge ($\omega = 1190.5\text{ cm}^{-1}$). As shown in Figure 5b, the edge fringe

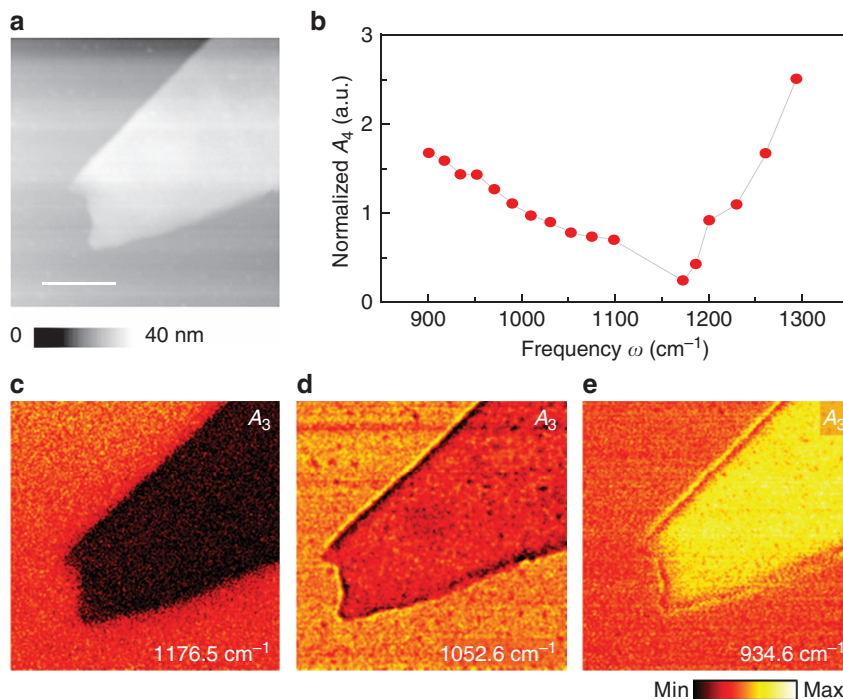


Figure 3 Near-field spectroscopic amplitude images of BP. (a) Topographic image and (c–e) 4th harmonic near-field amplitude images of BP on a SiO₂ substrate showing the evolution of the fringe contrast at three different frequencies. (b) Plot of the 4th harmonic normalized near-field amplitude contrast as a function of frequency. For a, scale bar = 200 nm.

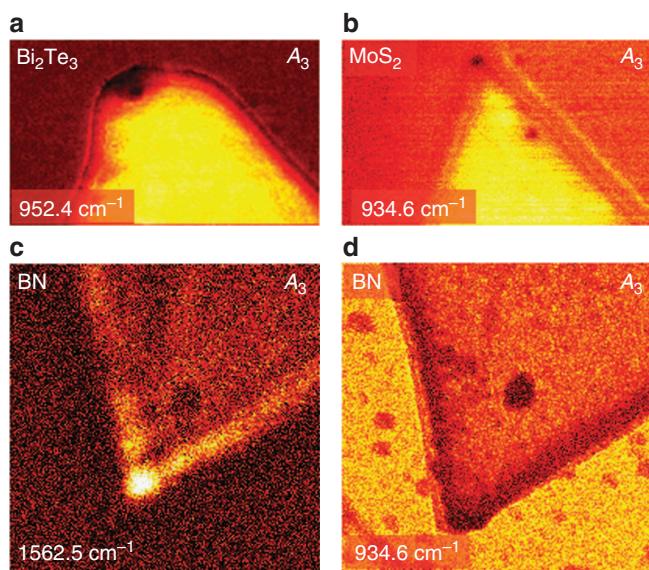


Figure 4 Near-field spectroscopic amplitude images of van der Waals layered nanofilms. (a) Topological insulator Bi₂Te₃, (b) semiconductor MoS₂ and (c, d) insulator h-BN of 100 nm in thickness c at a phonon–polariton range frequency of $\omega = 1562.5 \text{ cm}^{-1}$ and d outside the phonon–polariton range at $\omega = 934.6 \text{ cm}^{-1}$.

around the nanostructure is either weak or absent at $\omega = 934.6 \text{ cm}^{-1}$, whereas it is strong at this frequency in non-degraded samples. We attribute this change to alteration of the surface properties due to degradation, causing the surface to lose its metallic behavior. We note, however, that the surface near the edges of the sample degrades last, as indicated by the bright amplitude contrast at $\omega = 934.6 \text{ cm}^{-1}$

(Figure 5b), which turns to a darker contrast at $\omega = 1190.5 \text{ cm}^{-1}$ (Figure 5c). Based on the spectroscopic normalized amplitude plots of degraded and non-degraded BP, we can identify the bright portion shown in Figure 5b as relatively intact BP and the large darker region as degraded BP.

One of the fundamental questions in 2D materials science is the dependence of their physical properties on their thickness. To elucidate this dependence for the plasmonic properties of BP, we developed a procedure for its exfoliation using the electrostatic interaction with the s-SNOM tip biased at a potential difference ΔU with respect to the BP surface.

In Figure 6, we show the results of an exfoliation experiment. The topographic image in Figure 6a shows a nanoflake exfoliated at $\Delta U = 0 \text{ V}$; it indicates the position of a line profile taken at a nanoflake thickness of 39.5 nm. The corresponding near-field image is shown in Figure 6c, and it clearly shows the expected external fringe around the nanoflake. By contrast, Figure 6b shows a nanoflake exfoliated at $\Delta U = 15 \text{ V}$ and the position of a line profile taken in the region of the nanoflake with a thickness of 3.9 nm. The corresponding near-field amplitude image in Figure 6d does not show any discernible outside fringe; moreover, the pronounced bright contrast characteristic of plasmonic behavior is absent. Note that some dark spots are present in Figure 6d, likely caused by degradation (oxidation). For comparison, in Figure 1d and 1f, the degradation is more severe, yet the outside fringes are clearly seen. Thus, the absence of metallic behavior in Figure 6d is unlikely to be related to this partial degradation.

Therefore, our results suggest that the surface metallic nanolayer in BP disappears when the thickness decreases from ~ 10 to $\sim 4 \text{ nm}$. This finding is also consistent with ref. 9, in which it was found that only BP nanofilms with a thickness of $< 7.5 \text{ nm}$ were usable as

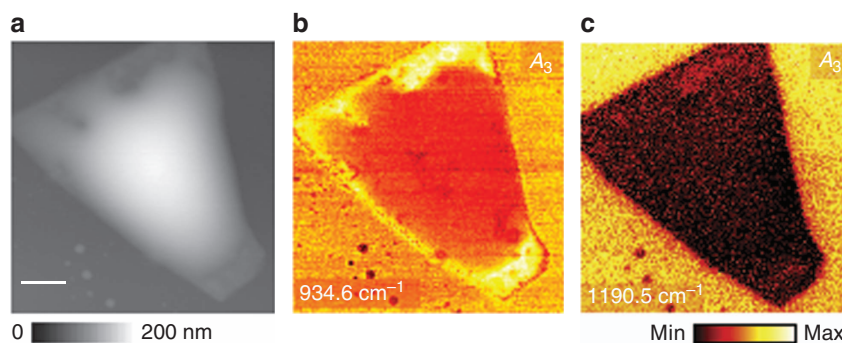


Figure 5 Near-field nanoscopic amplitude images of degraded BP. Third-harmonic near-field amplitude images of BP at two selected wavelengths showing the evolution of the optical contrast in oxidized BP. (a) Topography. (b) Near-field amplitude (A_3) at laser frequency of 934.6 cm^{-1} and (c) 1190.5 cm^{-1} .

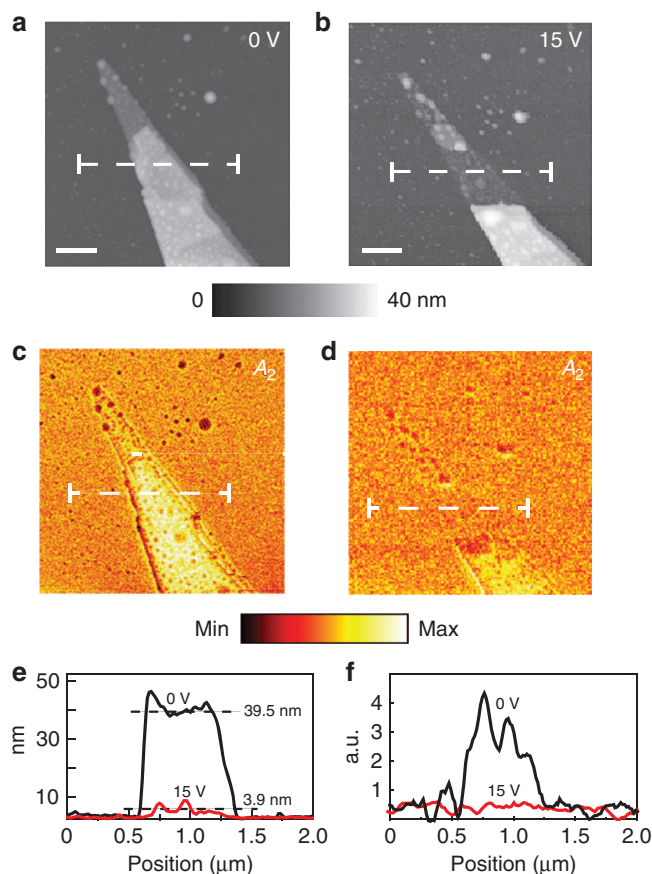


Figure 6 Exfoliation of BP by means of the s-SNOM tip potential. (a) Topography of an exfoliated BP nanoflake for $\Delta U=0\text{ V}$. The position of acquisition of the line profile is indicated by the dashed line. (b) Same as a but for $\Delta U=15\text{ V}$. (c) Near-field A_2 s-SNOM image of the nanoflake whose topography is shown in a. (d) The same as c but for the nanoflake shown in b. (e) Line profiles corresponding to the topographic images in a, b. (f) Line profiles corresponding to the near-field amplitude images in c, d.

semiconductor materials in the channels of FETs; the surface metallic layer of a thicker film would screen the gate field and prevent the FET from functioning. The corresponding line scans, shown in Figure 6e for topography and in Figure 6f for near-field amplitude, quantify the dependence on the BP thickness discussed above.

CONCLUSIONS

To conclude, we have shown the first experimental evidence that BP exhibits highly polarizable surface-metallic (plasmonic) behavior in the mid-IR frequency region, as revealed in the near field by the formation of an outside edge fringe. This behavior occurs only at frequencies below a certain threshold plasmon frequency, found to be $\omega_m \approx 1176\text{ cm}^{-1}$, which suggests a high-carrier concentration of $n \sim 10^{20}\text{ cm}^{-3}$ in the surface layer that results in metallic properties of the surface layer. The thickness of the metallic surface layer can be estimated from the Thomas–Fermi screening radius to be $\sim 1\text{ nm}$. This metallic behavior is likely the result of surface charges due to dangling bonds at the surfaces, a phenomenon that is well-known in bulk semiconductors but has been observed here for nanolayered materials for the first time; it is absent in a dielectric nanolayered material, h-BN.

BP shows promise as a semiconductor material in nanoelectronic devices, particularly FETs^{9,14,15}, in which its conductivity would be controlled by the gate field. For such applications, the observed presence of a metallic nanolayer at the surface is of primary importance because this metallic nanolayer would screen the gate field and prevent gate control for thicker samples—see the corresponding discussion in the previous paragraph. An understanding of the fundamental properties of BP as a nanoelectronic material is of fundamental importance for its potential applications in nanoelectronics. The conducting surface nanolayer of BP can be used for interconnects or for source and drain electrodes. The conductivity of the surface nanolayer can potentially be controlled by means of chemical or field-effect doping for the fabrication of planar transistors; note that the first transistor was created using spontaneous surface doping³⁶. BP is also promising for applications in nano-optics as a controllable nanoplasmonic material and in optoelectronics, particularly in high-speed compact electro-optical modulators.

CONFLICT OF INTEREST

The authors declare no conflict of interest.

AUTHOR CONTRIBUTIONS

YA and SG performed the experiments. MIS, YA, SBC and HW discussed the results. LZ, SBC and HW fabricated the samples. VB, MHJ and MIS performed the theoretical work and the numerical simulations. YA and MIS wrote the text of the paper.

ACKNOWLEDGEMENTS

YA acknowledges support by the National Science Foundation CAREER award under grant no. 1553251. SG acknowledges partial support provided by a grant from the Air Force Office of Scientific Research (AFOSR) grant no.

FA9559-16-1-0172. Work of MIS was supported by grant no. DE-SC0007043 from the Materials Sciences and Engineering Division of the Office of the Basic Energy Sciences, Office of Science, US Department of Energy. Work of VB was supported by MURI grant no. N00014-13-1-0649 from the US Office of Naval Research, and MHJ was supported by grant no. DE-FG02-01ER15213 from the Atomic, Molecular and Optical Sciences Program, Office of the Basic Energy Sciences, Office of Science, US Department of Energy. The work at USC was supported by DOE award no. DEFG02-07ER46376 (ZL) and NSF award no. 1402906 (SBC).

- Xia FN, Wang H, Xiao D, Dubey M, Ramasubramanian A. Two-dimensional material nanophotonics. *Nat Photonics* 2014; **8**: 899–907.
- Novoselov KS, Geim AK, Morozov SV, Jiang D, Katsnelson MI *et al*. Two-dimensional gas of massless dirac fermions in graphene. *Nature* 2005; **438**: 197–200.
- Novoselov KS, Fal'ko VI, Colombo L, Gellert PR, Schwab MG *et al*. A roadmap for graphene. *Nature* 2012; **490**: 192–200.
- Eckmann A, Park J, Yang HF, Elias D, Mayorov AS *et al*. Raman fingerprint of aligned graphene/h-bn superlattices. *Nano Lett* 2013; **13**: 5242–5246.
- Wang QH, Kalantar-Zadeh K, Kis A, Coleman JN, Strano MS. Electronics and optoelectronics of two-dimensional transition metal dichalcogenides. *Nat Nanotechnol* 2012; **7**: 699–712.
- Britnell L, Ribeiro RM, Eckmann A, Jalil R, Belle BD *et al*. Strong light-matter interactions in heterostructures of atomically thin films. *Science* 2013; **340**: 1311–1314.
- Ye ZL, Cao T, O'Brien K, Zhu HY, Yin XB *et al*. Probing excitonic dark states in single-layer tungsten disulphide. *Nature* 2014; **513**: 214–218.
- Liu XZ, Galfsky T, Sun Z, Xia FN, Lin EC *et al*. Strong light-matter coupling in two-dimensional atomic crystals. *Nat Photonics* 2015; **9**: 30–34.
- Li L, Yu Y, Ye GJ, Ge Q, Ou X *et al*. Black phosphorus field-effect transistors. *Nat Nanotechnol* 2014; **9**: 372–377.
- Low T, Roldán R, Wang H, Xia FN, Avouris P *et al*. Plasmons and screening in monolayer and multilayer black phosphorus. *Phys Rev Lett* 2014; **113**: 1068021–1068025.
- Favron A, Gaufrès E, Fossard F, Phaneuf-L'Heureux AL, Tang NY *et al*. Photooxidation and quantum confinement effects in exfoliated black phosphorus. *Nat Mater* 2015; **14**: 826–832.
- Lam K-T, Guo J. Plasmonics in strained monolayer black phosphorus. *J Appl Phys* 2015; **117**: 113105.
- Youngblood N, Chen C, Koester SJ, Li M. Waveguide-integrated black phosphorus photodetector with high responsivity and low dark current. *Nat Photonics* 2015; **9**: 247–252.
- Xia FN, Wang H, Jia YC. Rediscovering black phosphorus as an anisotropic layered material for optoelectronics and electronics. *Nat Commun* 2014; **5**: 4458.
- Koenig SP, Doganov RA, Schmidt H, Neto AHC, Ozyilmaz B. Electric field effect in ultrathin black phosphorus. *Appl Phys Lett* 2014; **104**: 1031061–1031064.
- Low T, Avouris P. Graphene plasmonics for terahertz to mid-infrared applications. *ACS Nano* 2014; **8**: 1086–1101.
- Tran V, Yang L. Scaling laws for the band gap and optical response of phosphorene nanoribbons. *Phys Rev B* 2014; **89**: 245407.
- Tran V, Soklaski R, Liang YF, Yang L. Layer-controlled band gap and anisotropic excitons in few-layer black phosphorus. *Phys Rev B* 2014; **89**: 235319.

- Du YC, Liu H, Deng YX, Ye PD. Device Perspective for Black Phosphorus Field-Effect Transistors: Contact Resistance, Ambipolar Behavior, and Scaling. *ACS Nano* 2014; **8**: 10035–10042.
- Jing Y, Tang Q, He P, Zhou Z, Shen PW. Small molecules make big differences: Molecular doping effects on electronic and optical properties of phosphorene. *Nanotechnology* 2015; **26**: 095201.
- Dai J, Zeng XC. Bilayer phosphorene: Effect of stacking order on bandgap and its potential applications in thin-film solar cells. *J Phys Chem Lett* 2014; **5**: 1289–1293.
- Rodin AS, Carvalho A, Castro Neto AH. Strain-induced gap modification in black phosphorus. *Phys Rev Lett* 2014; **112**: 176801.
- Reich ES. Phosphorene excites materials scientists. *Nature* 2014; **506**: 19.
- Eda G, Maier SA. Two-dimensional crystals: managing light for optoelectronics. *ACS Nano* 2013; **7**: 5660–5665.
- Zhang Z, Yates JT. Band bending in semiconductors: Chemical and physical consequences at surfaces and interfaces. *Chem Rev* 2012; **112**: 5520–5551.
- Kim J, Baik SS, Ryu SH, Sohn Y, Park S *et al*. Observation of tunable band gap and anisotropic dirac semimetal state in black phosphorus. *Science* 2015; **349**: 723–726.
- Stockman MI. Nanoplasmonics: past, present, and glimpse into future. *Opt Express* 2011; **19**: 22029–22106.
- Guler U, Boltasseva A, Shalaev VM. Refractory plasmonics. *Science* 2014; **344**: 263–264.
- Amarie S, Keilmann F. Broadband-infrared assessment of phonon resonance in scattering-type near-field microscopy. *Phys Rev B* 2011; **83**: 045404-045401–045404-045409.
- Fei Z, Andreev GO, Bao WZ, Zhang LFM, S McLeod AS *et al*. Infrared nanoscopy of dirac plasmons at the graphene-SiO₂ interface. *Nano Lett* 2011; **11**: 4701–4705.
- Jia YC, Zhao H, Guo QS, Wang XM, Wang H *et al*. Tunable plasmon-phonon polaritons in layered graphene-hexagonal boron nitride heterostructures. *ACS Photonics* 2015; **2**: 907–912.
- Stockman MI, Faleev SV, Bergman DJ. Localization versus delocalization of surface plasmons in nanosystems: can one state have both characteristics? *Phys Rev Lett* 2001; **87**: 167401–167404.
- Apalkov V, Stockman MI. Proposed graphene nanopaser. *Light Sci Appl* 2014; **3**: e191, doi:10.1038/lsa.2014.72.
- Dai S, Fei Z, Ma Q, Rodin AS, Wagner M *et al*. Tunable phonon polaritons in atomically thin van der Waals crystals of boron nitride. *Science* 2014; **343**: 1125–1129.
- Wood JD, Wells SA, Jariwala D, Chen KS, Cho E *et al*. Effective passivation of exfoliated black phosphorus transistors against ambient degradation. *Nano Lett* 2014; **14**: 6964–6970.
- Bardeen J, Brattain WH. The transistor, a semi-conductor triode. *Phys Rev* 1948; **74**: 230–231.



This work is licensed under a Creative Commons Attribution-NonCommercial-ShareAlike 4.0 International License. The images or other third party material in this article are included in the article's Creative Commons license, unless indicated otherwise in the credit line; if the material is not included under the Creative Commons license, users will need to obtain permission from the license holder to reproduce the material. To view a copy of this license, visit <http://creativecommons.org/licenses/by-nc-sa/4.0/>

© The Author(s) 2016

Supplementary Information for this article can be found on the *Light: Science & Applications*' website (<http://www.nature.com/lsa>).